JOURNAL OF GEOPHYSICAL RESEARCH, VOL. 103, NO. D22, PAGES 28,975–28,991, NOVEMBER 27, 1998

A distributed thermal model for calculating soil temperature profiles and depth of thaw in permafrost regions

Larry D. Hinzman, Douglas J. Goering, and Douglas L. Kane
Water and Environmental Research Center, University of Alaska, Fairbanks

Abstract. A spatially distributed thermal model has been developed that simulates thermal processes at the surface of the tundra, within the active layer, and in the underlying permafrost. This model was developed and applied to simulate processes on the Kuparuk River watershed on the North Slope of Alaska. Gridded meteorological data came from seven stations. Meteorologic data to calculate the surface energy balance at each of the nodes were distributed across the watershed using kriging. The kriged air temperature was also adjusted to account for elevation differences using the dry or wet adiabatic lapse rate as appropriate, and incident shortwave radiation was adjusted to consider slope effects. The equations describing the thermal processes of the surface energy balance were solved simultaneously for the surface temperature. This calculated surface temperature was then used in the subsurface finite element formulation to calculate the temperature profile and depth of thaw in the soil. Thermal properties of the soil were estimated spatially on the basis of measurements collected in typical landform vegetation units and then distributed on the basis of a vegetation map. Performance of the model was judged on the basis of comparison to measurements of soil temperatures and thaw depths. The model performs quite well in areas where subsurface thermal properties are well known. The model explains greater than 80% of variance at the surface when comparing predicted subsurface temperatures versus measured soil temperatures, and it increases in performance at greater depths. The model explains 82% of variance when comparing predicted thaw depths versus thaw depths measured over 1 km^2 grids.

1. Introduction

Accounting for the processes associated with energy and mass transfer is the cornerstone of most climatic and hydrologic studies in Arctic regions. Understanding the interaction of the thermal and hydrologic regimes is important; especially in the active layer (the thin layer of soil above the permafrost that experiences annual freeze/thaw). Almost all biologic and hydrologic processes occur on or within the active layer. In order to characterize hillslope hydrologic processes such as runoff or subsurface storage, it is necessary to quantify the thickness of the active layer as it increases throughout the thaw season. Biological processes such as root respiration and organic soil decomposition are strongly controlled by the active layer temperature and moisture content; carbon dioxide and methane fluxes are also functions of these active layer variables [*Vourlitis and Oechel,* 1998]. Our objective was to develop a model that could accurately predict the thickness of the active layer throughout the year over broad spatial scales.

2. Background

There were several modeling studies [*Nakano and Brown,* 1972; Ng and Miller, 1974; *Goodwin and Outcalt,* 1975; *Ng and Miller,* 1977] conducted in the 1970s in the Alaskan Arctic which identified and solved many of the problems associated with thermal analyses over permafrost. Additional modeling studies in this area have been completed recently, primarily in response to concerns over climatic change [*Bonan,* 1991; *Kane et al.,* 1991; *Waelbroeck,* 1993; *Waelbroeck et al.,* 1997].

In our complementary and concurrent effort to develop a model of Arctic hydrologic processes [*Hinzman et al.,* 1995], it was also necessary to develop an accurate model of surface and subsurface heat transfer processes across the same spatial and temporal domain. This thermal model has been designed to complement the hydrologic model described by Zhang et al., [1998], which, when complete, will provide distributed soil moisture values on compatible time increments. A future research effort will dynamically couple both models. Thermal analyses that we previously conducted in this area have identified numerous problems that we had to overcome. Work toward this goal began with the application of a heat conduction/phase change model called TDHC (two-dimensional heat conduction) [*Goering and Zarling,* 1985]. The subsurface model was driven by measured surface temperature and was able to simulate the daily thermal fluctuations and the seasonal active layer dynamics very well [*Kane et al.,* 1991]. This model suffered from a limitation that arose during simulations of a warming climate; as large masses of permafrost began to thaw, the thermal gradients would approach zero, as the permafrost became isothermal around the phase change temperature of 0°C. The lack of a significant gradient across numerous elements created an instability in the phase change algorithm, which was based on the dirac delta function method [*O'Neill,* 1983]. When the phase change is spread over a significant spatial extent, the delta function method typically identifies multiple phase change interfaces which, in turn, leads to instability.

Paper number 98JD01731.
0148-0227/98/98JD-01731$09.00

Thermal analyses were extended to include hydrologic processes in simulations which in essence were a quasi-static coupling of the HBV hydrologic model [*Bergström,* 1976] and the TDHC model [*Hinzman and Kane,* 1992]. Although these efforts acknowledged the importance of coupling thermal and hydrologic variables, these processes were simulated separately and the output linked to estimate the effect of changing climate upon such processes as runoff and evapotranspiration.

An effort was made to integrate the coupled behavior of thermal and hydrologic processes in a simulation of thermokarst development [*Hinzman et al.,* 1997]. During these efforts, a one-dimensional subsurface heat transfer model was formulated utilizing an apparent heat capacity method to include phase change [*Pradeep,* 1994]. In this approach, latent heat release is spread over a temperature range using an exponential function in order to approximately model the impact of unfrozen soil moisture at temperatures below 0°C [*Andersland and Anderson,* 1978]. This method is numerically more stable than the dirac delta function method used in the TDHC model, which attempts to identify a discrete phase change interface. The subsurface model described here was also driven by surface temperature, but in this case, the effective surface temperature was calculated by solving a system of equations representing the surface energy balance. This one-dimensional solution was then adapted to a quasi-three dimensional simulation by *Li* [1996] on the basis of the model presented here. This approach is described as a quasi-three-dimensional simulation because it consisted of a two-dimensional analysis across the topographic surface using surface energy balance simulations to calculate surface temperature and then subsurface one-dimensional thermal simulations were executed at each node, extending vertically into the active layer and permafrost.

A different approach to estimating spatially distributed thaw depths for approximately the same study area and time period as the simulations described in this paper was presented by *Nelson et al.* [1997]. Their technique, which consisted of solving the Stefan equation across the model domain through the application of a geographical information system (GIS), yielded good results.

3. Modeling Approach

Previous research [*Kane et al.,* 1991] has shown that the subsurface thermal dynamics may be simulated quite accurately if the surface temperature is provided and the soil thermal properties are known. Our approach in this study was to use distributed meteorologic data to calculate the surface temperature at a regular array of surface nodes spanning a large area (>28,000 km^2). The effective surface temperature was calculated for each node by solving the surface energy transfer equations simultaneously. This value of effective surface temperature was then used to drive the subsurface thermal model to calculate the temperature profile and depth of thaw.

3.1. Surface Energy Balance

Developing an estimate of the surface temperature across the model spatial domain proved to be a difficult task. The surface temperature is the most important variable in the solution of the surface energy balance equation as each of the interacting processes of the surface energy balance maintains a dynamic equilibrium with fluxes controlled by the magnitude of the surface temperature (Figure 1).

The surface energy balance may be written as:

$$Q_h + Q_e + Q_{net} + Q_c + Q_m = 0 \quad (1)$$

where Q_h is sensible heat flux between the surface and the air associated with convection, W/m^2; Q_e is latent heat flux associated with evaporation (sublimation or condensation), W/m^2; Q_{net} is energy transferred at the surface by net radiation, W/m^2; Q_c is energy flux via conduction between the soil surface and the subsurface, W/m^2; and Q_m is energy utilized for melting of the snowpack, W/m^2.

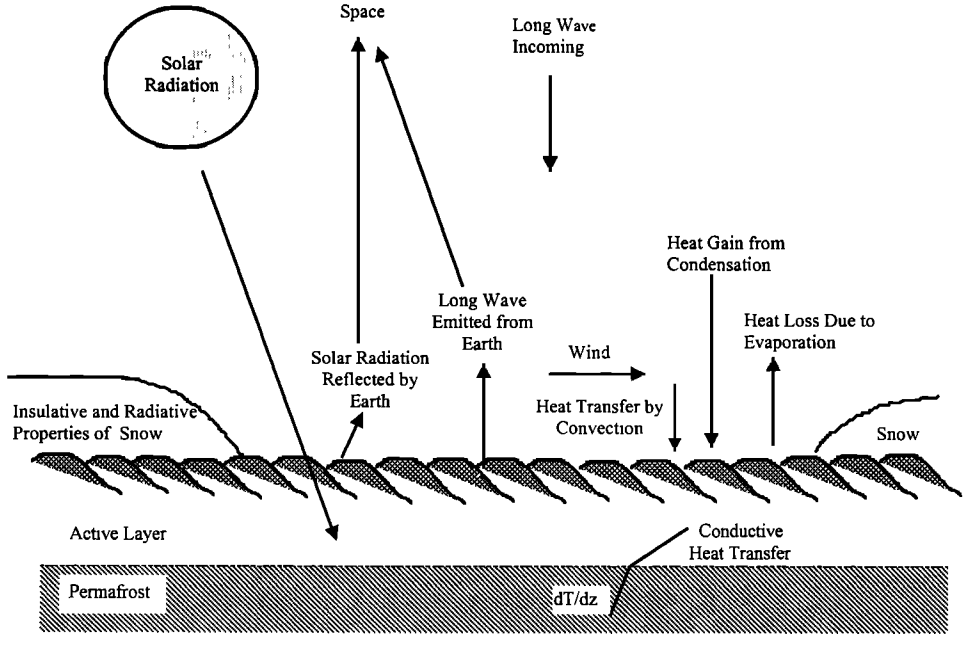

Figure 1. Schematic of surface energy balance and the processes included in the model solution for determining surface temperature.

Each equation that describes a single component of the surface energy balance includes the surface temperature as a variable. These can be assembled into a single nonlinear equation for the surface temperature. At each time step, this equation was generated using measured meteorological data and then solved for the surface temperature. Initially, the solution of this equation was carried out by Newton-Raphson iteration. However, because of intermittent (albeit rare) failures of the Newton-Raphson technique, we also incorporated a convergence checker and a bisection algorithm which was used as needed. In all cases the surface temperature error was driven to less than 10^{-4} °C before the sequence was terminated. The resulting surface temperature was then used as a boundary condition for the subsurface model when calculating thaw depth and soil temperatures.

The simulations carried out in this study were initiated after the spring snowmelt was completed. Although snow events can occur on any day of the year in Arctic Alaska, the heat transfer processes associated with snowmelt were neglected in this version of the model. Neither have the heat transfer processes associated with lateral water movements been incorporated in the model to date. Flux was arbitrarily defined as positive towards the surface.

Sensible heat transfer from the surface due to wind movements is nearly always significant on the North Slope of Alaska. This term can be measured directly with eddy correlation instrumentation; however, because of limitations in our equipment, we calculated this flux on the basis of wind speed and air temperature gradients [*Braun,* 1985]:

$$Q_h = C_p \rho_a D_{h(n,s,u)} (T_a - T_{sur}). \quad (2)$$

where C_p is specific heat of air at constant pressure, J/kg °C; ρ_a is density of air, kg/m^3; $D_h(n,s,u)$ is heat exchange coefficient, m/s (n= neutral, s = stable, and u = unstable) ;T_a is temperature of the air at height z, °C; and T_{sur} is temperature of the surface, °C.

Evaporation Q_e was calculated on the basis of the amount of soil moisture available near the surface. In this case, our approach differs from previous studies that have used a potential evapotranspiration which is then modified by an increasing stomatal resistance as conditions dry out [*Bonan,* 1991]. Instead, in this model, the actual specific humidity of the soil is used, but the vapor exchange coefficient is not altered for changing conditions:

$$Q_e = L_v \rho_a D_w (q_a - q_s) \quad (3)$$

where L_v is latent heat of vaporization of water, J/kg; D_w is vapor exchange coefficient, m/s; q_a is specific humidity of air at height z, kg/kg; and q_s is specific humidity at the surface, kg/kg.

The specific humidity may be calculated on the basis of the vapor pressure:

$$(q_a - q_s) = (0.622/p_{atm})(e_a - e_s) \quad (4)$$

where e_a is vapor pressure at height z, hPa; e_s is vapor pressure at the surface, hPa; and p_{atm} is atmospheric pressure, hPa.

The air vapor pressure in equation (4) is calculated from the relative humidity, *RH* data, as follows:

$$e_a = e_a RH \quad (5)$$

where e_{as} = saturation vapor pressure at temperature T_a, hPa; and *RH* = relative humidity (fraction).

The saturation vapor pressure can be computed with great accuracy from the following equations [*Brutsaert,* 1982]:

$$e_{as} = 101325 \exp (13.3185 t_R - 1.9760 t_R^2 - 0.6445 t_R^3 - 0.1299 t_R^4) \quad (6)$$

$$t_R = 1 - (373.15/(T_a + 273.15)) \quad (7)$$

The *RH* of air is easily measured, while the *RH* of the air at the soil surface may be calculated [*Campbell,* 1985] thus:

$$RH = \exp (M_w \psi / R\theta) \quad (8)$$

where M_w is the mass of a mole of water, kg/mol; ψ is water potential, J/kg; R is the Universal gas constant, (8.3143 J/mol K) ; and θ is temperature, K.

The water potential ψ is obtained from a measured characteristic curve (Figure 2) for the surface organic moss layer using a soil water suction apparatus in the laboratory on soils collected in the study area [*Hinzman et al.,* 1991b]. The extraction pressure is typically reported in terms of pascals, which can be related to soil water potential in J/kg. In this fashion, ψ can be related to the moisture content of the surface organic mat. During dry conditions the surface moisture content may decrease, resulting in reduced ψ and *RH* and thus a reduced Q_e. Optimal application of this thermal model would include temporal and spatial variability in soil moisture levels; however, in the simulations presented here, the moisture content remained constant for every time step but varied for each landscape type throughout the spatial domain.

Calculation of the convective heat transfer term Q_h and the evaporative heat transfer term Q_e was based on the assumption that the heat and vapor exchange coefficients D_h and D_w are equal to the momentum exchange coefficient D_m [*Szeicz et al.,* 1969]. A relationship that holds for neutral (isothermal) atmospheric conditions can be written as

$$D_{h(n)} = D_{w(n)} = \frac{u_z k^2}{\left[\ln (z/z_o)\right]^2} \quad (9)$$

where $D_{h(n)}$ is heat exchange coefficient for neutral atmospheric conditions, m/s; $D_{w(n)}$ is vapor exchange coefficient for neutral atmospheric conditions, m/s; k is the von Kàrmàn constant, 0.41; u_z is wind speed at height z, m/s; z is height of wind speed and temperature measurement, m; and z_o is average surface roughness, m.

It is possible to introduce some effect of vegetation on convective and evaporative heat transfer by varying surface roughness as a function of vegetation type; however, this level of complexity is not justified in a thermal model that calculates heat transfer on a 1 km nodal spacing. For nonneutral conditions, a correction must be applied to account for the stability of the air just above the ground surface [*Price and Dunne,* 1976]. To compensate for air stability, daily heat exchange coefficients were adjusted on the basis of the air temperature profile between the surface and the reference height z, using $D_{h(s)}$ for stable, and $D_{h(u)}$ for unstable conditions [*Braun,* 1985]. This was accomplished by comparing the air temperature T_a at height z with the simulated surface temperature T_s. If T_s was less than T_a, then the stable heat transfer coefficient was used:

$$D_{h(s)} = D_{h(n)}/(1 + 10 Ri) \quad (10)$$

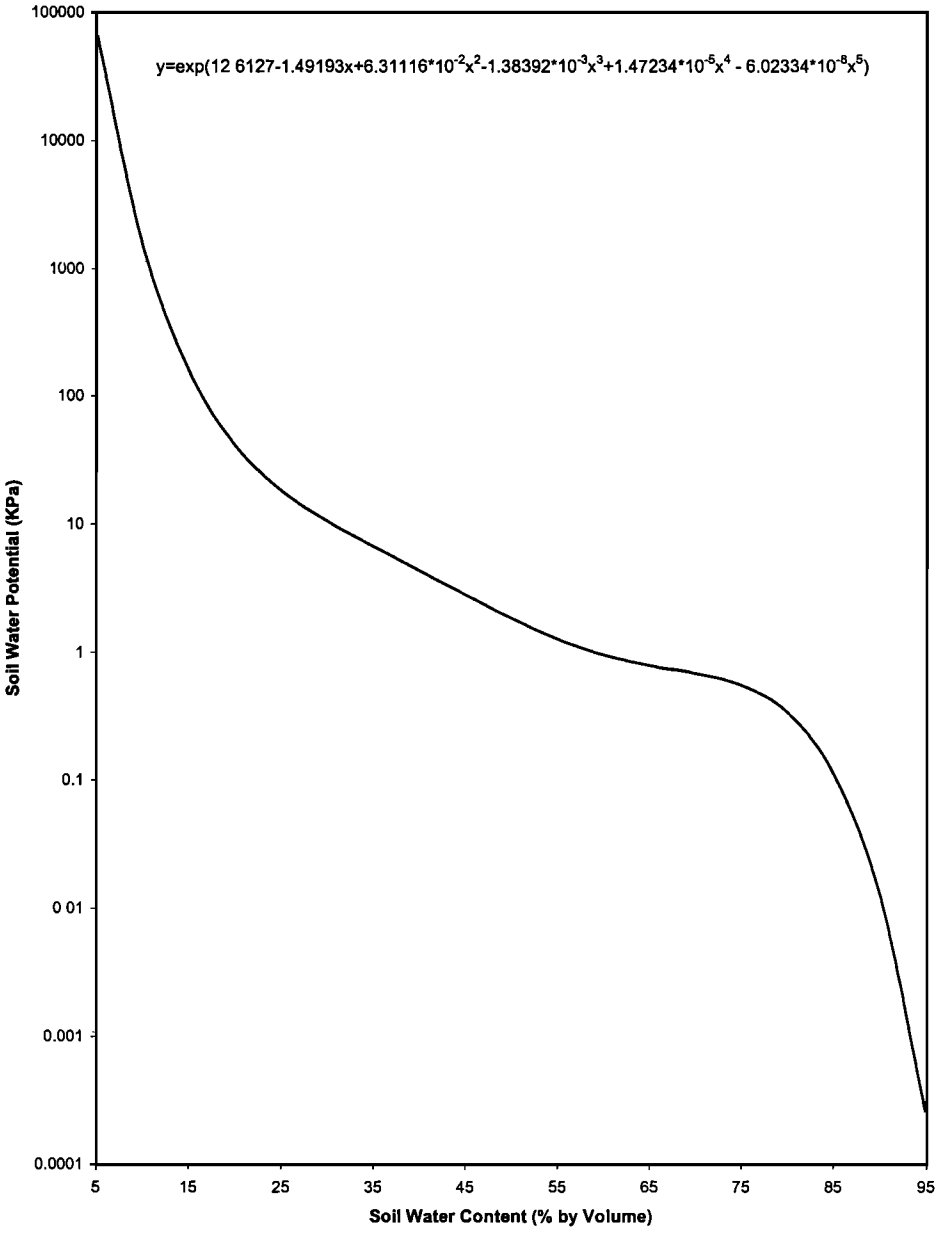

Figure 2. Parameterized soil-water characteristic curve for near-surface highly organic soils typical of arctic tundra (data from *Hinzman et al.* [1991b]).

where *Ri* is the Richardson Number, defined as

$$Ri = \frac{gz(T_a - T_s)}{u_z^2(T_a + 273.15)} \quad (11)$$

where g is the gravitational constant, m/s^2; T_a is the temperature of the air at height z, °C; and T_s is the temperature of the surface, °C.

When the air density at the surface is less than the air density above the surface, an unstable situation occurs and the heat transfer coefficient is calculated thus:

$$D_{h(u)} = D_{b(u)}(1 - 10\,Ri) \quad (12)$$

The net radiation Q_{net} is one of the primary driving model input variables and is measured at each meteorologic station. The energy conducted into the soil, Q_c, may be calculated from the Fourier heat conduction equation:

$$Q_c = K\,dT/dz \quad (13)$$

where K is the soil thermal conductivity, W/m °C; and d*T*/dz is the near-surface thermal gradient, °C/m.

Application of this equation is based upon the assumption of a linear thermal gradient across a 5 cm thickness of soil.

3.2. Subsurface Thermal Model

The subsurface thermal analysis is based on the solution of the unsteady one-dimensional conduction equation:

$$C_{app}\frac{\partial T}{\partial t} = \frac{\partial}{\partial z}\left(K\frac{\partial T}{\partial z}\right) \quad (14)$$

where C_{app} is apparent volumetric soil heat capacity, J/m^3 °C, T is soil temperature, °C; t is time, s; and z is spatial coordinate in vertical direction, m.

Table 1. Thermal Properties of Surface Organic Layer for Various Landscape Types and for Deeper Subsurface Soils, Assumed Constant Across Spatial Domain

	Landform Type	Thickness of Layer, m	Frozen Thermal Conductivity, W/m °C	Thawed Thermal Conductivity, W/m °C	Thawed Heat Capacity, * J/m³ °C	Frozen Heat Capacity, J/m³ °C	Latent Heat, J/m³
Layer 1							
	Barren	0.50	0 54	0.39	4.86E+05	9 91E+05	4.24E+07
	moist acidic tundra	0.15	0 58	0.38	1.24E+06	8.11E+05	5.00E+07
	moist nonacidic, dry tundra	0.10	0.81	0.43	1.64E+06	1.31E+06	4.92E+07
	shrublands	0 20	0.58	0 34	1.24E+06	8.11E+05	5 00E+07
	wet tundra	0.30	0.64	0.47	1 14E+06	1.25E+06	4 76E+07
	water	0.50	3 85	1.24	3.23E+06	4.89E+06	3.35E+08
Layer 2		0 80	2.05	1 5	3.70E+05	5.90E+05	2.50E+08
Layer 3		18 - 19**	3.63	1.69	2 64E+06	4.22E+06	2.50E+08

* Read 4.86E+5 as 4.86×10^5.

** Depends upon thickness of surface layer, but total thickness is equal to 20 m.

The thermal conductivity K, the latent heat L, and the soil heat capacity C_s were distributed (across the spatial domain and depth) based on a vegetation/landform map [*Auerbach and Walker,* 1995], utilizing physical properties measured in the field in characteristic landform types (Table 1). Values of K, L, and C_s were estimated on the basis of soil properties using procedures described by *Zarling et al.* [1989]. Estimated values of K were validated with comparisons of thermal conductivity analyses of samples taken from the Kuparuk watershed [*Hinzman et al*, 1991b].

In general, the thermal gradient and heat transport in the horizontal direction is several orders of magnitude smaller than the corresponding vertical component. Consequently, the model considers only heat transport in the vertical direction. K and C_{app} may vary with moisture content and the thermal state of the soil (frozen or thawed). In addition, latent heat release due to phase change is included in C_{app}. These property variations result in a governing equation that is highly nonlinear, thus requiring a numerical solution. Boundary conditions for the model include the time-varying surface temperature generated by the surface energy balance and the geothermal heat flux of 0.05 W/m^2, which is applied at the base of the grid [*Osterkamp and Payne,* 1981].

A one-dimensional finite element formulation was used to descretize and solve equation (14). Simple linear elements of irregular size were used to construct the vertical grid (Table 2). Twenty nodes extending from the surface to approximately 11 m depth were utilized in the subsurface simulations. Eleven nodes were included within the top meter as this was the zone of the most dynamic thermal processes. Thermal property variations and coupling with the surface temperature were treated in an explicit fashion in conjunction with a small time step size to ensure accuracy.

In the arctic region of concern in this study, most of the seasonally varying heat flux at the ground surface interface produces freezing or thawing of the active layer soils. This is in contrast with the situation in more temperate climates where the ground surface heat flux primarily produces sensible temperature variations in the near-surface soils. Because of the added importance of latent heat due to freeze/thaw, we have formulated an adjustable model of the freeze/thaw process which allows us to include the effect of unfrozen soil moisture [*Pradeep,* 1994]. Not all of the water in a soil freezes immediately as the soil temperature progresses below 0°C. The unfrozen water content of the soil is reduced exponentially from 100% at 0°C to somewhere between 40% and 2% unfrozen at -10°C depending upon soil type, [*Anderson and Morgenstern,* 1973]. In many cases the soil temperature must fall several degrees below 0°C before substantially all of the soil water is in the frozen state. This results in a release of latent heat that may take place over a significant temperature range. Our model is based on a latent heat content function, which is formulated using a combination of exponentials:

Table 2. Node Number and Corresponding Soil Depth for Subsurface Finite Element Grid

Node	Depth, m
1	0.00
2	0.02
3	0 05
4	0 08
5	0.13
6	0.18
7	0.26
8	0.36
9	0.50
10	0.67
11	0 90
12	1.19
13	1 58
14	2 09
15	2.76
16	3.64
17	4.79
18	6.29
19	8.26
20	10.85

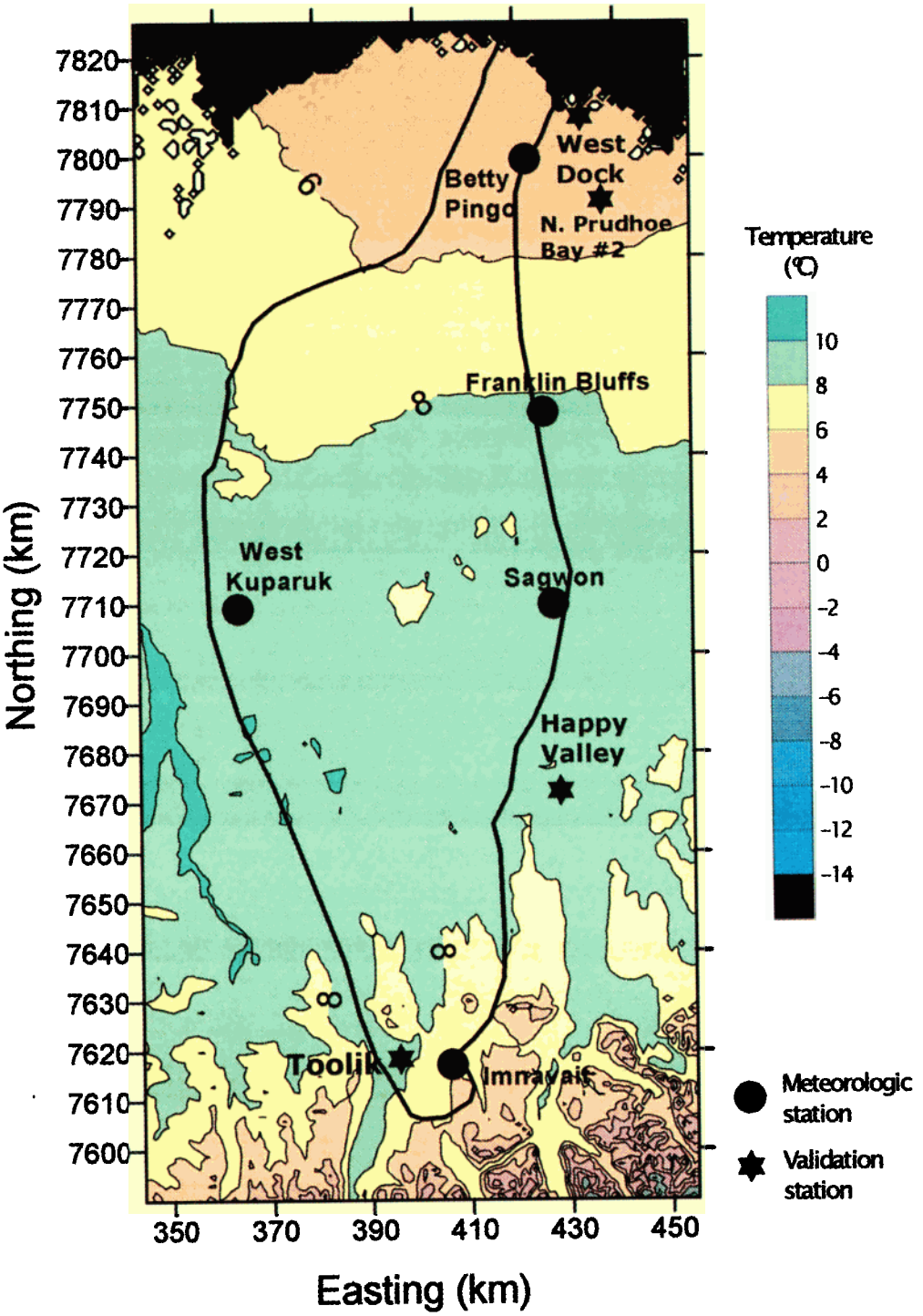

Plate 1. Spatially distributed air temperature (°C) on June 15, 1995 over the Kuparuk Basin. Air temperature was distributed on the basis of measurements at five meteorologic stations and adjusted for elevation using standard lapse rate.

$$LHC = L\frac{\exp\left(-\frac{pT}{\Delta T}\right) - \exp\left(-\frac{pT_{ll}}{\Delta T}\right)}{\exp\left(-\frac{pT_{hh}}{\Delta T}\right) - \exp\left(-\frac{pT_{ll}}{\Delta T}\right)} \quad (15)$$

where LHC is latent heat content of soil at temperature T, J/m^3; L is total latent heat released during freezing, J/m^3; p is adjustable constant; T is soil temperature, °C; T_{ll} is soil temperature when freezing is complete, °C; T_{hh} is soil temperature when freezing is initiated (usually = 0°C), °C; and ΔT is T_{hh} - T_{ll}.

This function results in a latent heat content that varies from 100% to 0% exponentially as the soil temperature drops from T_{hh} to T_{ll}. Figure 3 shows the resulting curves for the case where T_{hh} = 0°C, T_{ll} = -2°C, and p is varied from 1 to 10. The parameter p is determined by the soil type and must be selected by matching the generated curve with laboratory measurements of unfrozen water content versus temperature below freezing [*Farouki,* 1981].

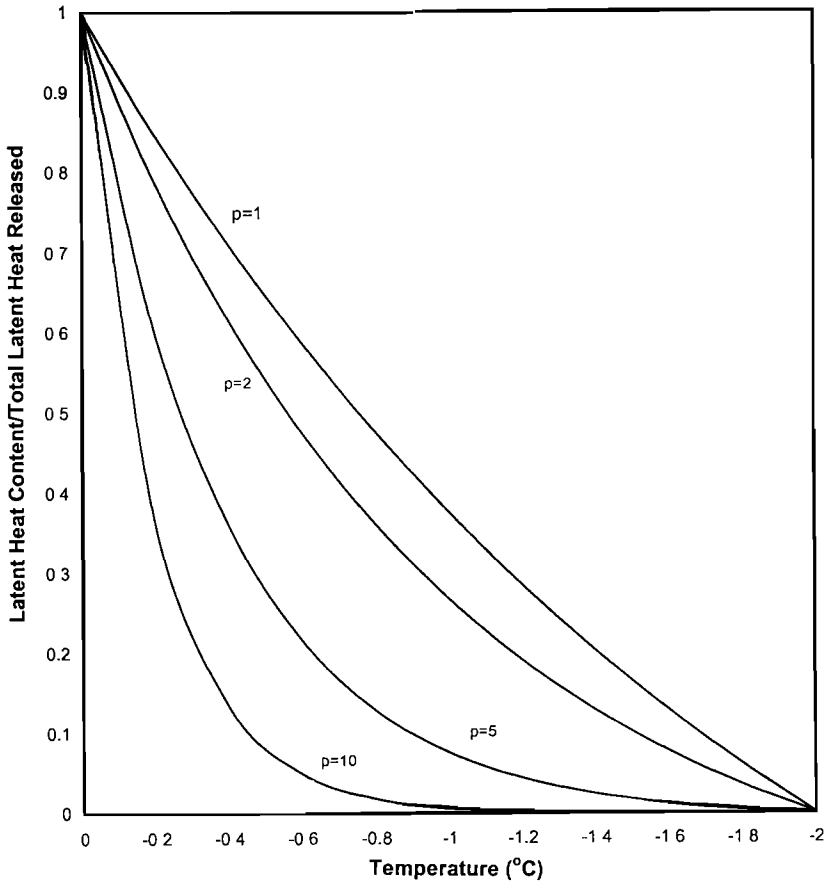

Figure 3. Latent heat curves for $\Delta T = 2°C$ with p varying from 1 to 10 (equation (15)).

Typically, the soil freezing curve of a coarse-grained soil such as sand could be represented with a p of 10 and to represent a fine grained soil such as a clay, one would select a p of 1. For the active layer soils of concern in the present study, we used values of 0°C and -2°C for T_{hh} and T_{ll}, respectively, and set p equal to 2. These values result in an unfrozen moisture content (or latent heat content) curve which closely matches experimental data for similar soil types as those encountered in this study [*Andersland and Anderson,* 1978]. Typically, T_{hh} would be affected by soil water content (i.e., for drier soils, T_{hh} would likely be less than 0°C); however, since these soils are always quite wet during freezing and thawing, it was valid to assume a uniform value for T_{hh}. The latent heat L released during freezing is a function of the water content of the soil. Again, in this simulation the water content was not allowed to vary dynamically; however, a static water content was estimated for each landform type based on field measurements (Table 1). Although the very near surface organic soils (in general, 0 – 20 cm) do vary broadly in moisture content during the summer, the subsurface soils (depths greater than 20 cm) do not vary much (10%) throughout the year [*Hinzman et al.,* 1991b]. This is due to the permafrost, which acts as a barrier to infiltrating water [*Kane and Hinzman,* 1988].

To include the latent heat contribution described above, the latent heat content function is differentiated with respect to temperature and included in the apparent heat capacity:

$$C_{app} = C_s + \frac{d(LHC)}{dT} \tag{16}$$

where C_s is sensible heat capacity of soil, J/m^3°C.

The above equation is used for the apparent heat capacity only for regions that have a temperature within the phase change zone ($T_{hh} < T < T_{ll}$). For regions with a temperature outside the phase change zone, the apparent heat capacity is set equal to the sensible heat capacity of the soil. C_{app} is included in the finite element integration such that the latent heat contribution is allotted proportionately to the layers that are located within or near the phase change zone.

4. Site Description

Permafrost is continuous under the entire study area, affecting landscape patterns, microclimatology, hydrologic processes, and thermal regime. The depth of the active layer ranges from 25 to ~100 cm. Typically, across the study area the top 0 to 20 cm of the soil profile is a highly porous organic soil with moisture contents that vary significantly (20 – 80% by volume) throughout the summer as controlled by local meteorological conditions [*Hinzman et al.,* 1991b]. The thickness of the organic layer ranges from less than 10 cm on ridge tops in the southern foothills to more than a meter in valley bottoms and in places on the northern coastal plain. The underlying mineral soils are usually saturated with water. Although driving and validation data were utilized from numerous sites across the model spatial domain, the site characteristics tend to vary most in a north/south direction. Therefore general site descriptions are only provided from selected sites in the three physiographic regions, foothills, transitional, and coastal plain.

The most southern site where meteorological data were

collected is Imnavait Creek (latitude 68°37' N, longitude 149°17' W, elevation 900 m, established 1985) in the northern foothills of the Brooks Range. The highly stratified soils, classified as Pergelic Cryaquepts or Histic Pergelic Cryaquepts [*Rieger et al.*, 1979], strongly influence both hydrologic and thermal regimes [*Hinzman et al.*, 1991b]. There is a thick, porous layer of organic matter on the surface, consisting of partially decomposed mosses, sedges, and other associated plants, which saturates and drains quickly.

A midregion site, Sagwon Bluffs, (latitude 69°25' N, longitude 148°45' W, elevation 370 m, established 1987) was installed approximately 100 km south of Prudhoe Bay. This site is located in a transitional zone between the coastal plain and the foothills. The vegetation is also characteristic of tussock tundra and the soils (Pergelic Cryaquepts) are loamy with a peaty surface layer and are poorly drained [*Everett*, 1980]. Instrumentation for measuring soil temperatures and meteorologic conditions were installed near the top of a 10% north-facing slope.

A more northern station was established on the coastal plain near Prudhoe Bay (latitude 70°18' N, longitude 148°55' W, elevation 15 m, established 1994) at the Betty Pingo site. This site is located in a wetland complex with little topographic relief. The vegetation consists of wet sedge tundra and forb tundra [*Rovansek et al.*, 1996]. The soils are organic overlying layers of fine sand and silts and have been classified as a complex of euic Pergelic Cryosaprists and Pergelic Cryohemists [*Ping et al.*, 1994].

5. Instrumentation Specifications

Campbell Scientific data loggers were used to record and process data at all sites. Data recorded on the data loggers were compared to field measurements to check the sensor calibrations. Meteorologic variables were measured once each minute. These measurements were averaged or totaled with output recorded once an hour. A 10 m meteorological tower was used to support the air temperature, relative humidity, wind speed, and direction sensors at two to three elevations. Radiation sensors were mounted on a separate tripod designed to suspend these sensors over the tundra and minimize shadows. Radiation sensors are operated from early spring until fall (about early April through September). All other sensors are operated throughout the year.

Air temperature and relative humidity were measured using a Campbell Scientific model 207 temperature and relative humidity probe. The relative humidity component utilizes a Phys-Chemical Research Corporation PCRC humidity transducer. These probes were housed in a self-aspirating radiation shield and are used at all sites. The suggested temperature operating range is -33 to +48°C with a worst case accuracy of 0.4°C and typical accuracy of 0.2°C, and 1°C accuracy from -33°C to -40°C. The relative humidity operating range is 12 to 100% with an accuracy of 5%. Soil temperatures were measured using YSI model 44007 thermistors and 100 K ohm precision resistors. The accuracy of these thermistors is rated at 0.2°C from 0° to 80°C. The accuracy declines below 0°C to 0.3°C at -25°C.

Radiation instruments were installed in the spring, usually during March or April, and were usually taken down in September. Since these are remote, unmanned sites, rime ice, snowfall, and freezing precipitation can coat the sensors in these instruments, especially the upper surface. The following radiation components were measured: incident and reflected shortwave radiation, atmospheric and terrestrial longwave radiation, photosynthetically active radiation and net radiation. Net absorbed radiation was measured with a REBS Q6 net radiometer. The radiation and energy balance systems (REBS) Q6 net radiometer spectral response range is reported by the manufacturer as 0.25 to 60 μm; the calibrated accuracy of this

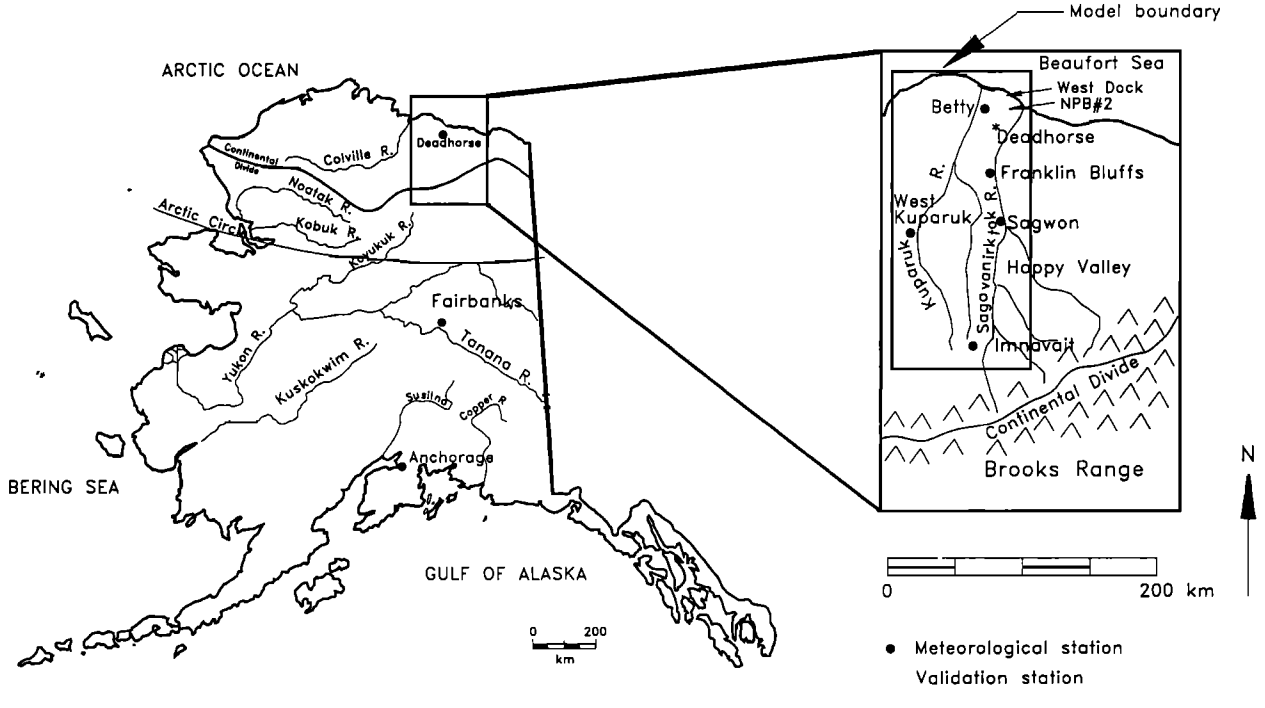

Figure 4. Region studied in these simulations includes the Kuparuk River basin and adjacent landscape on the North Slope of Alaska.

instrument was not reported by the manufacturer. Incident and reflected shortwave radiation was measured using an Eppley model PSP precision spectral pyranometer. This instrument has a reported spectral range of 0.285 to 2.800 μm and a reported accuracy of 0.5% between 0 and 2800 W/m^2. The cosine response of this instrument was 1% between 0° and 70° and 3% between 70° and 80° zenith angle. Eppley model PIR precision infrared pyrgeometers were used to measure longwave radiation, both terrestrial and atmospheric, at both sites. The spectral range of this type of instrument is 4 to 50 μm, and the accuracy is reported as 1% between 0 and 700 W/m^2.

6. Meteorological Data Areal Extrapolation

To simulate the active layer thermal dynamics across the spatial and time domains, it was necessary to create spatially distributed, time series data files of the important meteorologic variables and soil thermal parameters. To satisfy that need, we have attempted to develop algorithms which extend the meteorologic measurements collected at seven primary meteorologic stations (Imnavait Creek, Upper Kuparuk, Sagwon Bluffs, West Kuparuk, Franklin Bluffs, West Dock, and Betty Pingo) to yield measurements on a spatial grid. Figure 4 shows the location of these meteorologic stations with respect to the model boundary and the Kuparuk River basin. These data sets were quite large and difficult to manipulate; however, we were primarily interested in developing a more physically based model utilizing the necessary data as opposed to an empirical model, which may require lessor amounts of data. Data sets used included air temperature, relative humidity, wind speed, incoming shortwave radiation, and net radiation. The difficulty in utilizing a standard contouring routine to extrapolate data outward from the group of meteorologic stations is that the polynomial functions derived in the standard algorithms are not constrained at the edges of the grid. Consequently, the quality of the generated data is the poorest at the edge of the grid and best near meteorologic stations.

Our method of extrapolation depends on the variable in question. For example, air temperature varies spatially but also displays predictable variation with elevation. Air temperature data (Plate 1) were adjusted for elevation (range is sea level to 2145 m), using the dry (1°C/100 m) or moist (0.5°C/100 m) adiabatic lapse rate depending upon conditions. In this approach, the relative humidity was first estimated at each node by kriging among meteorological stations. If the relative humidity at a meteorological station was greater than 95%, the air temperature at that site was changed to sea level conditions using the moist adiabatic lapse rate. The sea level air temperature was then kriged across the spatial domain. These kriged values were then corrected for the elevation of each node, again using the appropriate wet or dry lapse rate. Net radiation (Figure 5) data were corrected for slope based on terrain and sun angle as described by *Hinzman et al.* [1992].

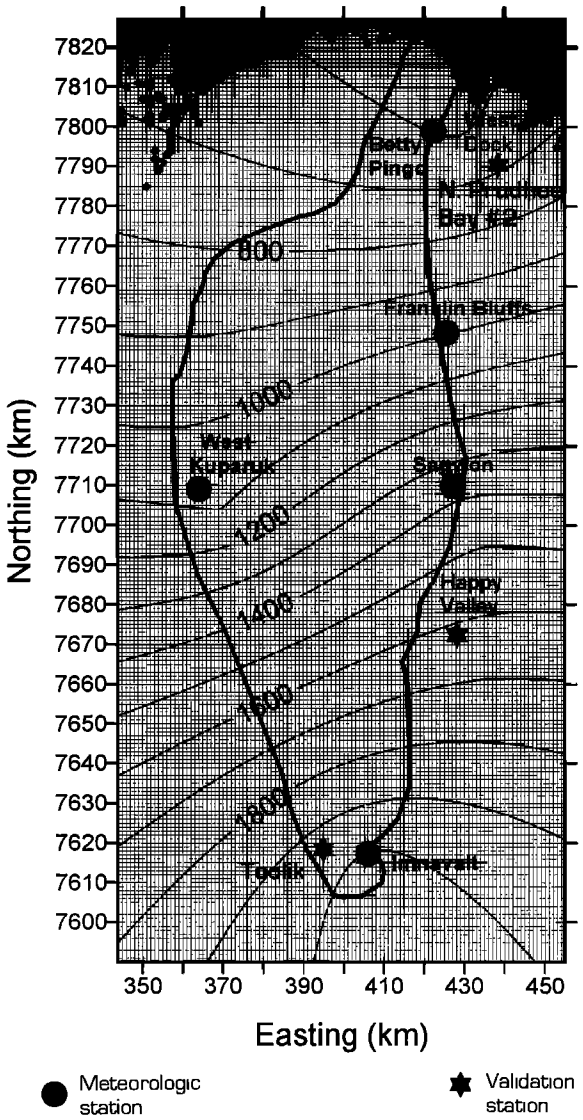

Figure 5. Spatially distributed daily total net radiation (W/m^2) on June 15, 1995, over the Kuparuk basin. Net radiation was not adjusted for small scale changes in cloudiness. The grid, with 26,656 nodes on 1 km spacing is also shown.

7. Distributed Thermal Simulations

The surface energy balance was simulated using a grid with 26656 nodes on a 1 km nodal spacing. Figure 5 shows the gridded area and the boundary of the Kuparuk watershed. At each node the one-dimensional (1-D) finite element program simulated the subsurface thermal dynamics to determine the temperature profile and depth of thaw. This 1-D nonuniform vertical grid had 20 nodes extending to a total depth of 20 m. A sequential program was written in Fortran and executed on the University of Alaska Arctic Regions Supercomputing Center's (ARSC) Cray YMP and SGI Onyx L. A parallelized version of the code has also been developed to run on the ARSC Cray T3D using up to 64 parallel processor elements. The simulation ran for 109 days, in 1 day time steps, and required 58 min on the Onyx L and 22 min on the T3D with 16 processing elements. Minimal run-time reduction was obtained with greater than 16 processor elements [*Li*, 1996]. Inefficiencies in data passing required in the surface energy balance routine of this version of the model limited the runtime reduction we were able to achieve with higher numbers of processor elements.

The thermal properties of the surface soils were distributed according to material properties measured in characteristic landscape types [J.G. Bockheim, unpublished data, 1997; C.L. Ping, unpublished data, 1997; and F.E. Nelson, unpublished data, 1997] and distributed on the basis of a map of vegetation

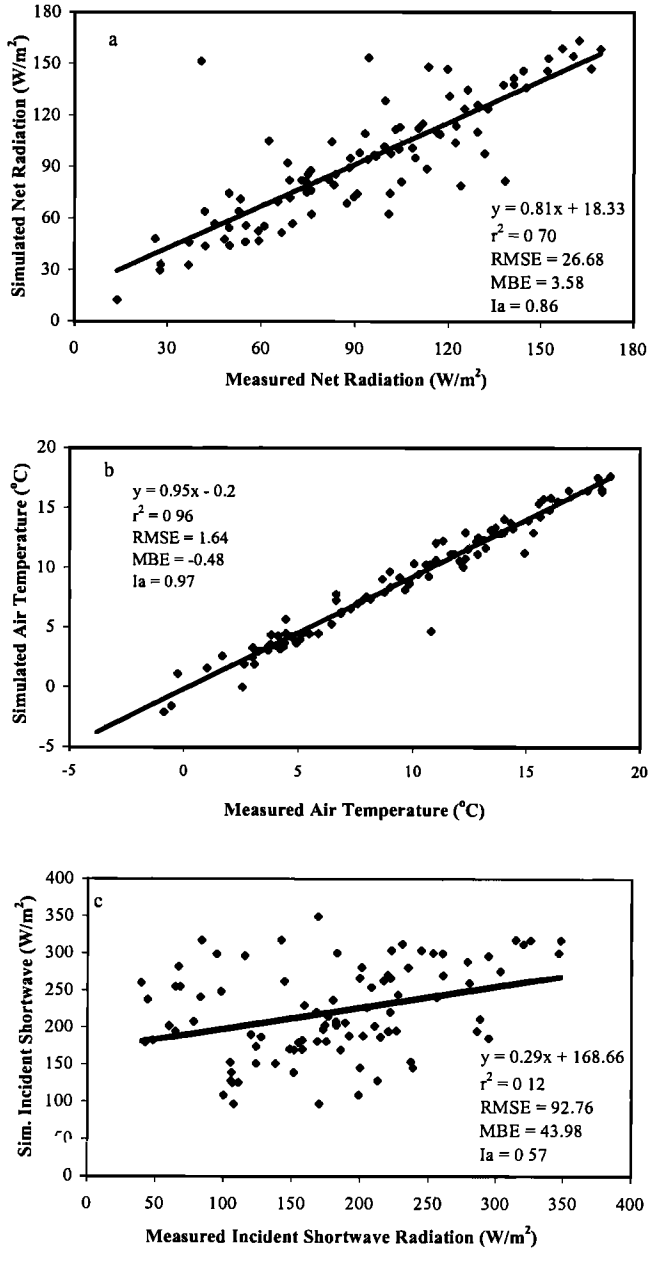

Figure 6. Comparison of mean daily measured and simulated meteorologic input data at Happy Valley site throughout the 1995 summer season: (a) net radiation, (b) air temperature, (c) incident shortwave radiation.

[*Auerbach and Walker,* 1995]. Table 1 lists the properties that were used in the thermal model for each of the six landform types. For each case, the thickness of the topmost layer varied according to type, as shown in column 1 of the table. The second and third layers were uniform in thermal properties regardless of landform type. Site-specific soil information is known, but no extensive soil survey data are available over the watershed within the Kuparuk River basin.

The thermal simulation was run for the Kuparuk watershed for the period May 15 to September 1, 1995, using 1 day time increments. Ground temperatures were initialized at the beginning of the simulation based on measured data. As the simulation progressed, subsurface temperatures and depth of thaw were calculated on a daily basis using the changing surface temperature as a driving boundary condition. Output variables include energy fluxes associated with evaporation, sensible heat, conduction into the soil, surface temperature, and depth of thaw at selected time points.

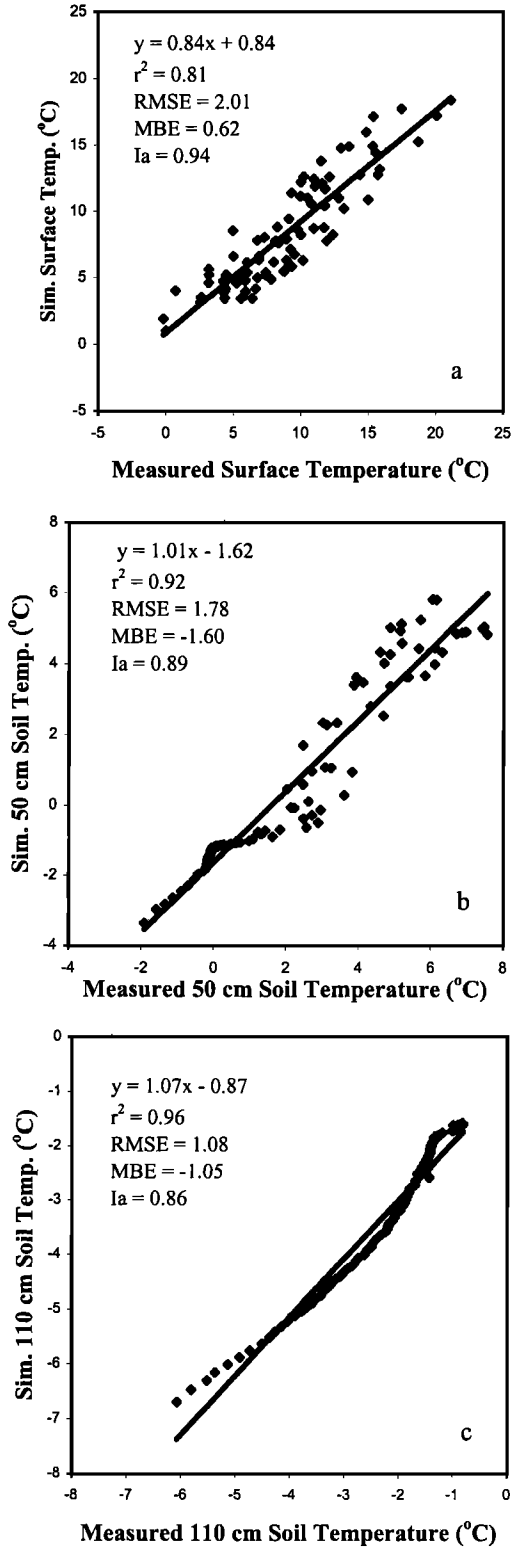

Figure 7. Comparison of mean daily measured and simulated soil temperatures at North Prudhoe Bay 2 throughout the 1995 summer season: (a) surface temperature, (b) 50 cm depth and (c) 110 cm depth.

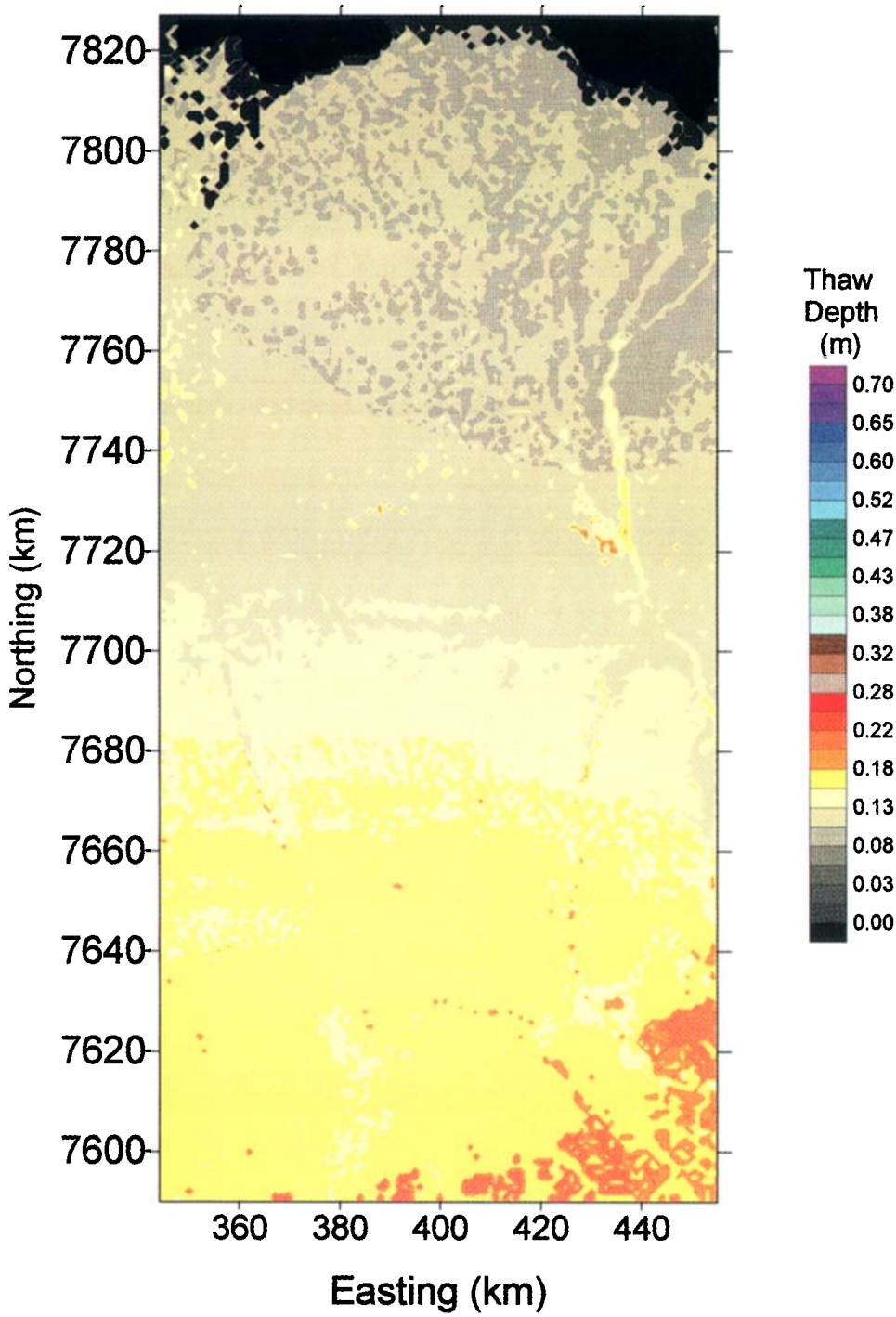

Plate 2. Simulated active layer depth across spatial domain on June 1, 1995.

8. Model Validation

Our modeling analyses include validation of thermal simulations and the distributed data used to drive the model. Each of these modeling exercises requires separate approaches and data sets to validate our simulated results. Although a large number of lakes and ponds exist in the northern portion of the Kuparuk basin, our input data were collected from meteorologic stations established in representative terrestrial areas. These lakes are only a significant presence in the northern 25% of the spatial domain but in that region can average 20% of the area. This does not influence the calculation of thaw depth in terrestrial areas.

One statistical method used to compare the performance of the model is a relative index of agreement (I_a) defined as [*Wilmott and Wicks*, 1980]

$$I_a = 1 - \left[\frac{\sum_{i=1}^{N} (P_i - O_i)^2}{\sum_{i=1}^{N} (|P_i - O_m| + |O_i - O_m|)^2} \right] \quad (17)$$

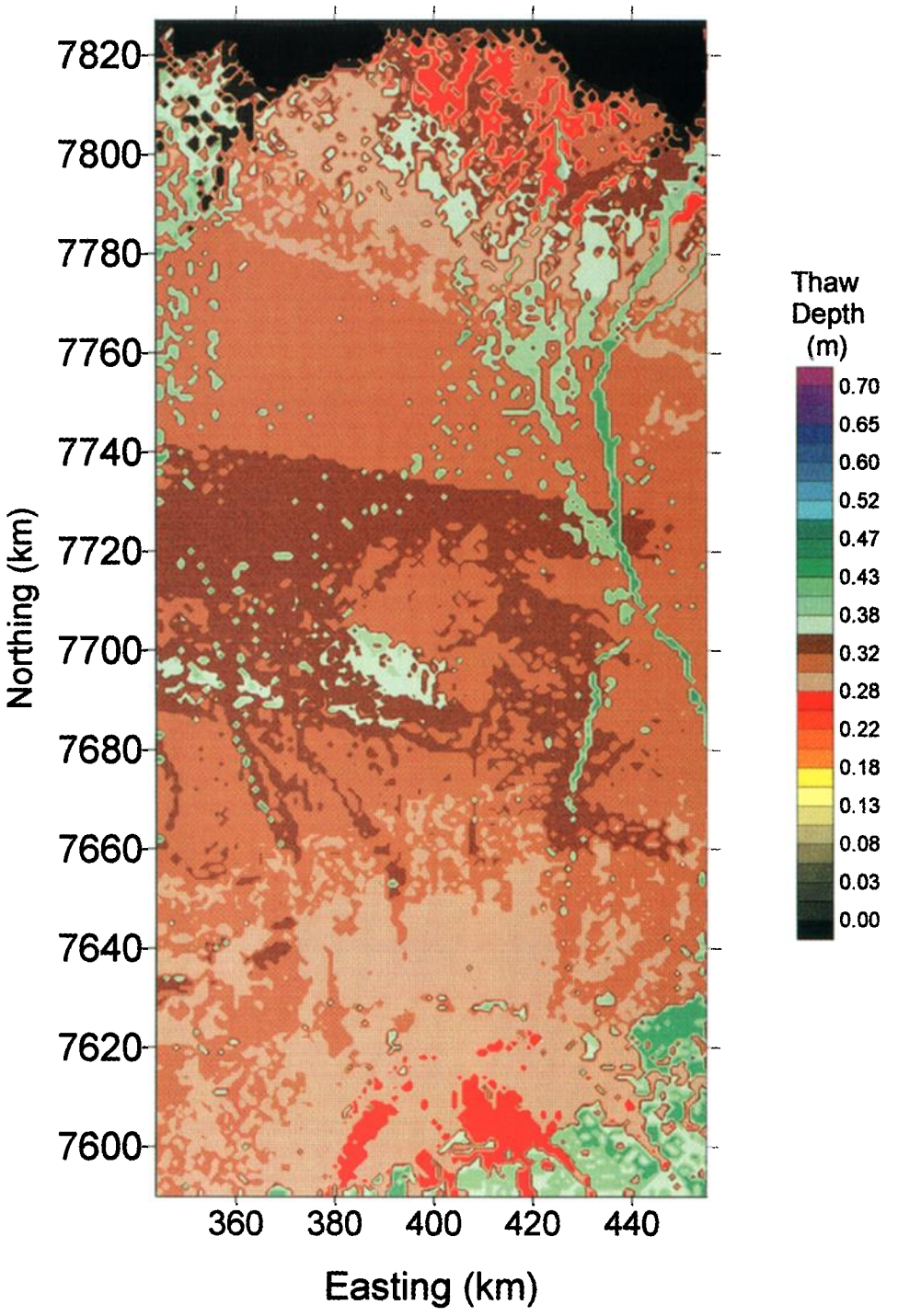

Plate 3. Simulated active layer depth across spatial domain on July 1, 1995.

where P_i and O_i are the predicted and observed values, respectively. O_m is the average observed value, and N is the number of data points used (i.e., number of days). This index has values ranging from 0 (worst performance) to 1 (best possible performance). The root mean square error (*RMSE*), which is a measure of nonsystematic error, and the mean bias error (*MBE*), which provides a measure of systematic error [*Halliwell and Rouse,* 1989], are also calculated to examine model performance. The *RMSE* and *MBE* as used by *Halliwell and Rouse* [1989] are similar in form to the population standard deviation and average population deviation from the mean [*Kitchens,* 1987]:

$$RMSE = \sqrt{\frac{\sum_{i=1}^{N} [P_i - O_i]^2}{N}} \tag{18}$$

$$MBE = \frac{\sum_{i=1}^{N} [P_i - O_i]}{N} \tag{19}$$

The *MBE* indicates whether a model underpredicts or overpredicts a variable throughout a given period of time, so if

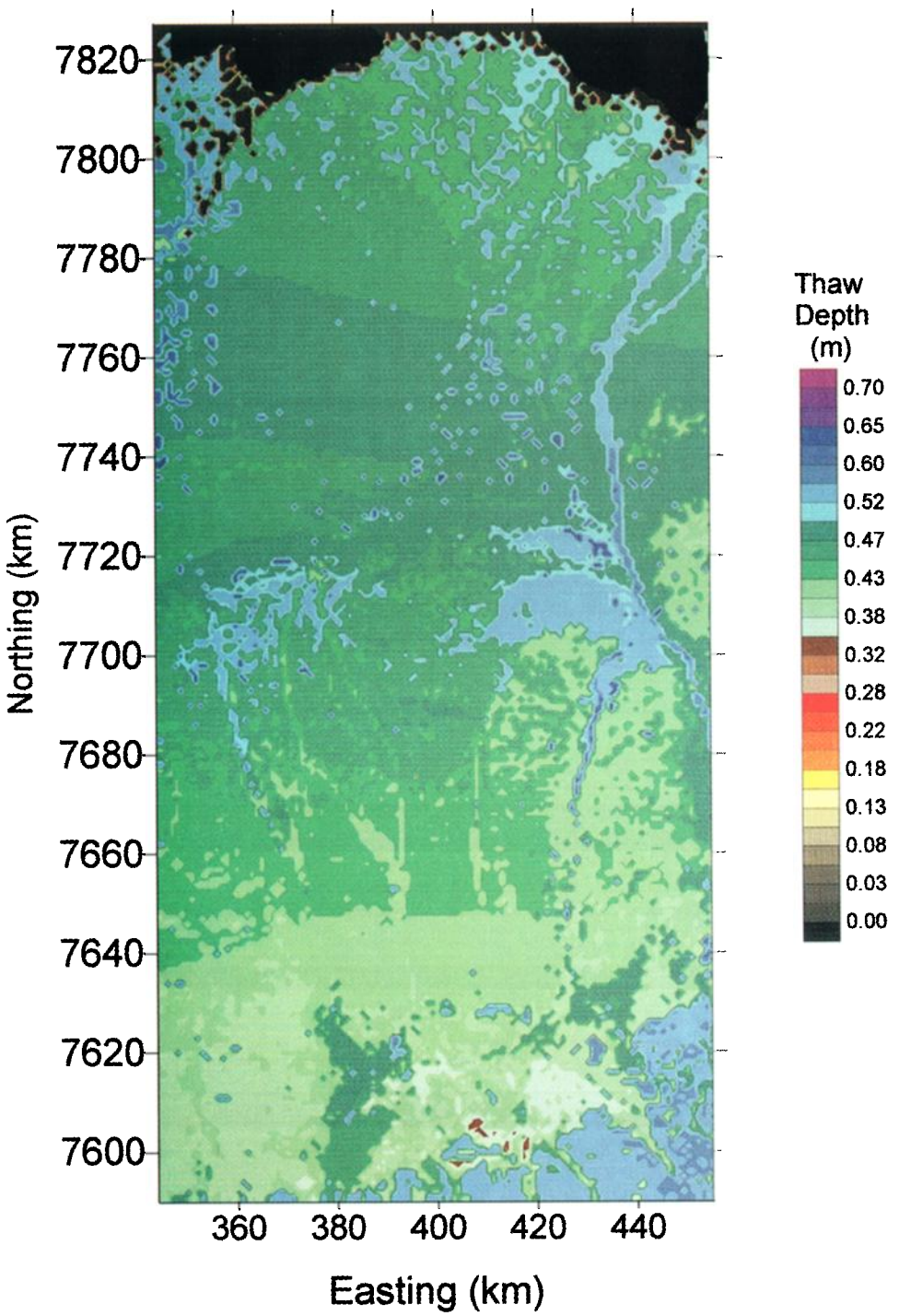

Plate 4. Simulated active layer depth across spatial domain on August 1, 1995.

the error is completely random, the *MBE* value will be zero. Whereas the *RMSE* gives a measure of the total error and does not distinguish between underprediction or overprediction since the difference between the predicted and the observed value is squared. Thus a zero *RMSE* means that there is no deviation between the predicted and the observed values.

The distributed meteorological data were compared to independent data collected near Happy Valley by *Vourlitis and Oechel* [1998]. These comparisons were quite favorable in most cases. Figures 6a, 6b, and 6c display comparisons of net radiation (r^2= 0.70, I_a = 0.86, *RMSE* = 26.68 W/m^2, *MBE* = 3.58 W/m^2), air temperature (r^2 = 0.96, I_a = 0.97, *RMSE* = 1.64 °C, *MBE* = -0.48 °C), and incoming shortwave radiation (r^2 = 0.12, I_a = 0.57, *RMSE* = 92.76 W/m^2, *MBE* = 43.98 W/m^2). Shortwave radiation displayed the greatest differences between modeled and measured values. This is probably due to the local effects of clouds as the differences decrease and the correlation of predicted versus measured increases as one averages over longer time periods.

Validation of the combined one-dimensional surface energy balance and subsurface heat transfer model was accomplished by comparing measured and simulated temperatures near Prudhoe Bay and Imnavait Creek. A total of five different land surface

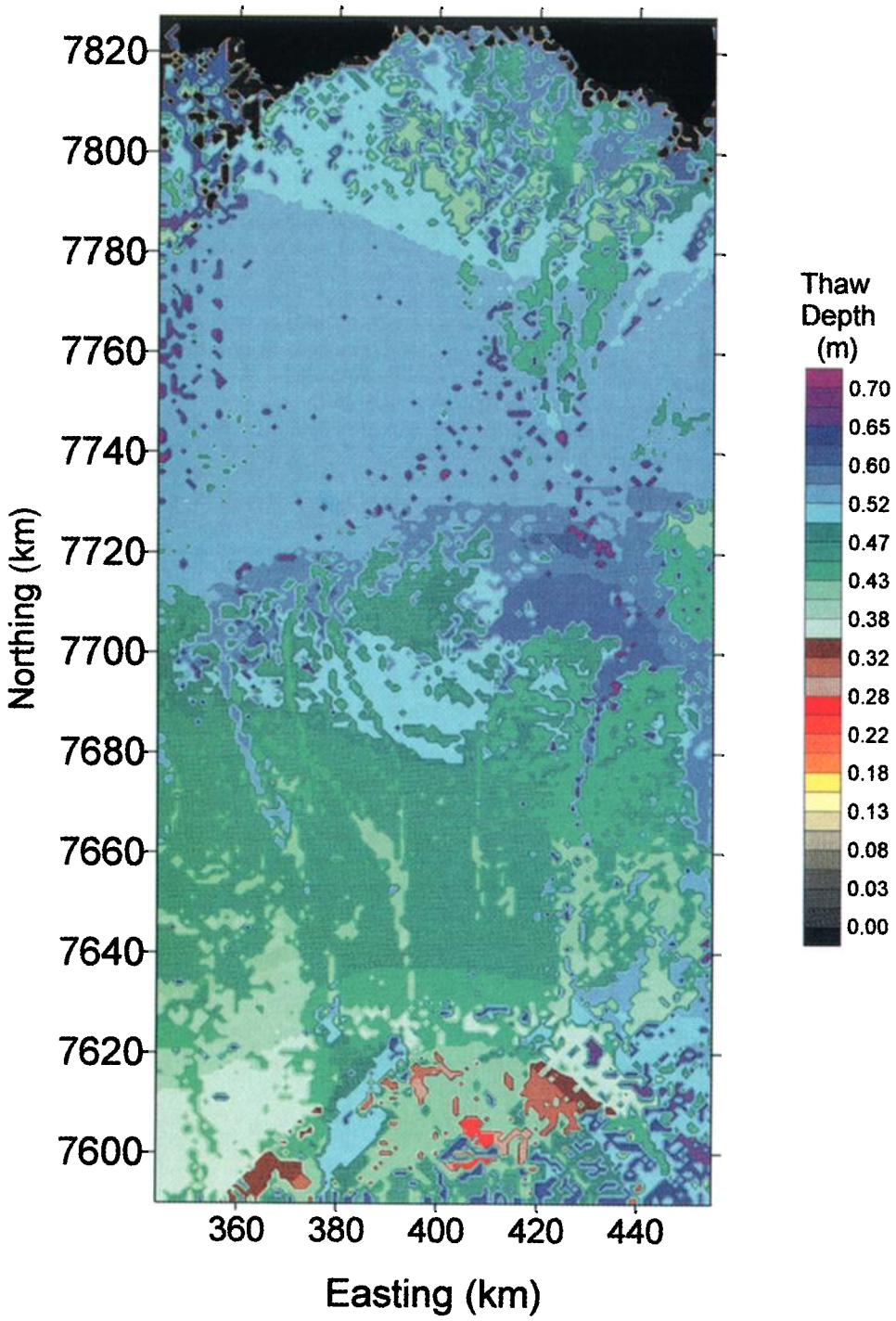

Plate 5. Simulated active layer depth across spatial domain on September 1, 1995.

types were examined. In each case we obtained good agreement between the measured and simulated temperatures. Figures 7a, 7b, and 7c show the comparison of the predicted versus measured surface and subsurface temperatures near Prudhoe Bay (site name is North Prudhoe Bay 2). Measured and simulated temperatures are compared at the surface and at two subsurface locations. In general, the measured and simulated temperatures agree to within a few degrees. Performance is better at greater depths, as some advective heat transfer, which is not included in model algorithms, does occur in the porous surface organic soils. In deeper, ice-rich soils, heat conduction is the dominant mechanism of heat transfer; while this is basically true in the near-surface soils, advective heat transfer by infiltration of snowmelt and rainfall are important for short periods of time. Note that the scatter of points in Figures 7a, 7b, and 7c decreases markedly below 0°C as advective heat transfer is almost nil in frozen soils. The numerical simulations were based on general thermal properties described in Table 1, rather than measured values taken from this specific site. Discrepancies at four other sites were similar to those shown in Figures 7a, 7b, and 7c. In spite of the natural variability of soil thermal properties, this demonstrates the capability of simulating thermal processes fairly well using general soil classifications.

Validation of the distributed active layer thermal simulations

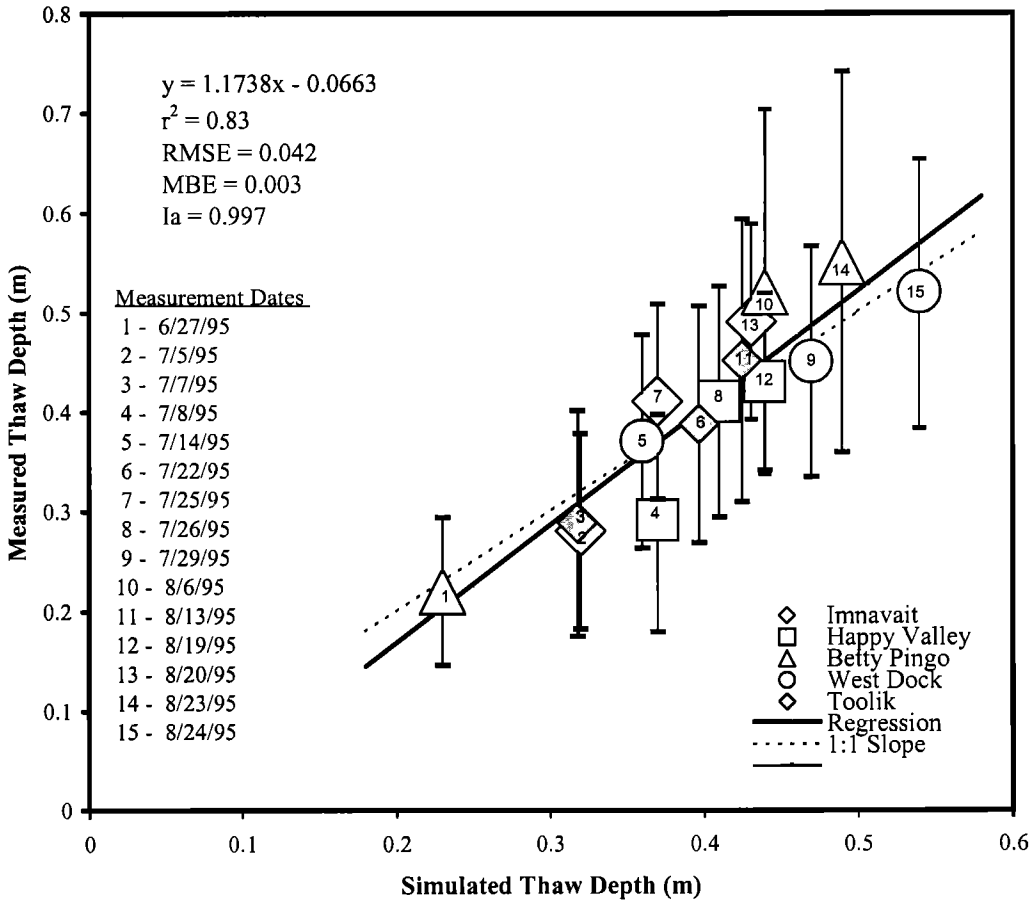

Figure 8. A comparison of simulated versus average measured thaw depths at five 1 km^2 sites at various times throughout the 1995 summer.

were based upon probe measurements collected periodically throughout the summer by members of our research group and those provided by F. Nelson's group (unpublished data, 1997). Five 1 km^2 grids were probed on 100 m increments (yielding 121 grid points) several times throughout the summer to determine the spatial and temporal variation in depth of thaw. The grid average at each site was compared to model simulations (Figure 8). These grids represent a north/south transect which traverses approximately 200 km from near the Arctic Ocean to the foothills of the Brooks Range, encompassing a variety of climatic conditions, substrate type, soil moisture conditions, and terrain. The depth of the thaw was measured multiple times (3-4) near each 100 m grid point, and the entire grid average was then compared to our simulation results. The model presented an adequate prediction of thaw depth at these five locations, each of which was measured three times during the summer of 1995 (r^2= 0.83, I_a = 0.997, *RMSE* = 0.042, *MBE* = 0.003). Optimum performance of the model would yield data points on a line with a slope equal to 1. The standard deviation of each measurement data set is included in Figure 8 as error bars about the mean of the measured thaw depth.

9. Results

Simulated thaw depths were generated over the entire computational domain extending from the foothills of the Brooks Range to the Arctic Ocean, an area of 250 by 120 km. We examined thaw depths periodically throughout the summer season to follow the progression of active layer development. Plates 2-5 show the simulated thaw depths for the entire domain on June 1, July 1, August 1, and September 1, respectively. These figures illustrate large differences in thaw depth within the region at any particular time as well as changes throughout the summer. These differences are due to regional variations in climatic conditions, soil thermal properties, and topography.

Plate 2 indicates that thawing of the active layer begins first in the southern portion of the domain corresponding to the northern foothills of the Brooks Range. Thawing then proceeds to the south into the Brooks Range and to the north on to the Coastal Plain as has been observed in previous field studies of snowmelt [*Hinzman et al.*, 1991a]. By July 1, thawing on the Coastal Plain has progressed to nearly the same extent as in the southern region (Plate 3). Later in the summer the variability in thaw depth throughout the domain increases significantly. Plates 4 and 5 show that the region encompassing the White Hills (the region spanning Northing 7700 km to 7760 km) has an enhanced thaw depth later in the season. Other (LAII) investigators have noted that differences in snow cover, carbon flux, and other land surface processes in this region probably related to differences in climatic conditions there as compared to other areas in the Kuparuk watershed. No grids were installed in that region, so we cannot

make direct comparisons of the model to measurements in the White Hills. Plate 5 represents the maximum depth of thaw and, consequently, the active layer thickness at the end of summer.

10. Conclusions

Quantifying the active layer thickness is critical in assessing hydrologic, biologic, and biogeochemical processes. The results presented here demonstrate a model for predicting this important characteristic of the Arctic landscape over large geographic regions. The model was validated through point comparisons at several sites representing the major landform types in the Kuparuk basin; however, it is anticipated that the model will be more useful in recreating regional trends rather than site-specific predictions. Predicted thaw depths display large variations throughout the basin, as would be expected from differences in climatic conditions and substrate properties. The results also show interesting trends in thaw depth development at different locations in the domain as the summer progresses. Maximum thaw depth is an important variable in many biological, hydrological, and engineering analyses, and therefore these results will be useful in related Arctic studies. This thermal model would also provide a useful tool for analyzing landscape evolution in a changing climate.

Acknowledgments. Programming and data processing assistance was provided by Elizabeth K. Lilly, Shu Li, and Robert E. Gieck and Water and Environmental Research Center graduate students. Soil property data, measured thaw depths, and vegetation data were provided by LAII cooperative investigators, including Fritz Nelson, Ken Hinkel, Jerry Brown, Jerry Mueller, Nickolai Shiklomanov, James Bockheim, C.L. Ping, Gary Michaelson, Donald Walker, and Nancy Auerbach. We would like to thank two anonymous reviewers whose insightful comments substantially improved the quality of this manuscript. Funding for this research was provided by the National Science Foundation under the Arctic System Science (ARCSS) Land Atmosphere Ice Interactions (LAII) Program (grants OPP-9214927 and OPP-9318535).

References

Andersland, O.B., and D.M. Anderson, *Geotechnical Engineering for Cold Regions,* McGraw-Hill, New York, 1978.

Anderson, D.M., and N.R. Morgenstern, Physics, chemistry and mechanics of frozen ground: A review, in *Proceedings of the Second International Conference on Permafrost,* pp. 257-288, Nat. Acad. of Sci., Washington, D. C., 1973.

Auerbach, N. A., and D. A. Walker, *Preliminary Vegetation Map, Kuparuk River Basin, Alaska: A Landsat-Derived Classification, Joint Facility for Regional Ecosystem Analysis,* Inst. of Arct. and Alp. Res., Univ. of Colo., Boulder, 1995.

Bergström, S., Development and application of a conceptual runoff model for Scandinavian catchments, Rep. RHO7, 118 pp., Swed. Meteorol. and Hydrol. Inst., Norrköping, Sweden, 1976.

Bonan, G.B., A biophysical surface energy budget analysis of soil temperature in the boreal forests of interior Alaska, *Water Resour. Res., 27*(5); 767-781, 1991.

Braun, L.N., Simulation of snowmelt-runoff in lowland and lower alpine regions of Switzerland, in *Zücher Geographische Schriften,* Vol. 21, 166 pp., Geogr. Inst., Eidg. Tech. Hochsch., Zürich, Switzerland, 1985.

Brutsaert, W., *Evaporation Into the Atmosphere, Theory, History, and Applications,* 299 pp., D. Reidel, Norwell, Mass, 1982.

Campbell, G.S., *Soil Physics With Basic: Transport Models for Soil-Plant Systems. Dev. in Soil Sci. 14,* 150 pp., Elsevier Sci., New York, 1985.

Everett, K.R. Soils and mapping, in *Environmental Engineering and Ecological Baseline Investigations Along the Yukon River-Prudhoe Bay Haul Road,* edited by J. Brown and R.L. Berg, pp. 48-52, CRREL Report 80-19, U.S. Army Cold Regions Research and Engineering Laboratory, Hanover, NH, 1980.

Farouki, O.T., Thermal properties of soils, CRREL Monogr. 81-1, 151 pp., Cold Reg Res. And Eng. Lab, Hanover, N.H., 1981.

Goering D.J., and J.P. Zarling, Geotechnical thermal analysis with a microcomputer, in Civil Eng. in the Arctic Offshore, pp. 604-616, Am. Soc. of Civ Eng., New York, 1985.

Goodwin, C.W., and S.I. Outcalt, The development of a computer model of the annual snow-soil thermal regime in arctic tundra terrain, in *Climate of the Arctic,* edited by G. Weller and S.A. Bowling, pp 227-229, Univ. of Alaska, Geophys. Inst., Fairbanks, 1975.

Halliwell, D.H., and W.R. Rouse, A comparison of sensible and latent heat flux calculations using the Bowen ratio and aerodynamic methods, *J. of Atmos. Oceanic Technol., 6,* 563-574, 1989.

Hinzman, L.D., and D.L. Kane, Potential response of an arctic watershed during a period of global warming, *J. of Geophys. Res. Atmos., 97;* 2811-2820, 1992.

Hinzman, L.D., D.L. Kane, and R.E. Gieck, Regional snow ablation in the Alaskan Arctic, in *Northern Hydrology, Selected Perspectives,* edited by T.D. Prowse and C.S.H Ommanney, pp. 121-140, Nat. Hydrol. Res. Inst., Saskatoon, Saskatchewan, 1991a.

Hinzman, L.D., D.L. Kane, C.S. Benson, and K.R. Everett, Hydrologic and thermal properties of the active layer in the Alaskan Arctic, *Cold Reg. Sci. and Technol., 19*(2), 95-110, 1991b.

Hinzman, L.D., G. Wendler, R.E. Gieck, and D.L. Kane, Snowmelt at a small Alaskan arctic watershed, 1, Energy related processes, in *Proceedings of the Ninth International Conference on Northern Research Basins,* edited by T.D. Prowse, C.S.L. Ommanney, and K. Ulmer, pp. 171-197, National Hydrology Research Institute, Saskatoon, Saskatchewan, Canada, 1992.

Hinzman, L.D., D.L. Kane, and Z. Zhang, A spatially distributed hydrologic model for arctic regions, in *International GEWEX Workshop on Cold-Season/Region Hydrometeorology,* Int. GEWEX Proj. Off. Publi. Ser., 15, pp. 236-239, Washington, D. C., 1995.

Hinzman, L.D., D.J. Goering, T C. Kinney, and S. Li. Numeric simulation of thermokarst formation during disturbance, in *Disturbance and Recovery in Arctic Lands: An Ecological Perspective,* edited by R.M.M. Crawford, pp. 191-211, Kluwer Acad., Norwell, Mass., 1997.

Kane, D L., and L.D. Hinzman. Permafrost hydrology of a small arctic watershed, in *Proceedings of the Fifth International Conference on Permafrost,* edited by K. Senneset, pp. 590-595, Tapir, Trondheim, Norway, 1988.

Kane, D.L., L.D. Hinzman, and J.P. Zarling. Thermal response of the active layer in a permafrost environment to climatic warming, *Cold Reg. Sci. and Technol., 19,* 111-122, 1991.

Kitchens, L., *Exploring statistics: a modern introduction,* 595 pp., West Publ., St. Paul, Minn., 1987.

Li, S., Development of parallel simulation software for the study of thermal processes in Kuparuk River basin of Alaska, 127 pp., M.S. thesis, Univ. of Alaska Fairbanks, 1996.

Nakano, Y., and J. Brown, Mathematical modeling and validation of the thermal regimes in tundra soils, Barrow, Alaska, *Arc. and Alp. Res.. 4*(1), 19-38. 1972.

Nelson, F.E., N.I. Shiklomanov, G.R. Mueller, K.M. Hinkel, D.A. Walker, and J.G. Bockheim, Estimating active-layer thickness over a large region: Kuparuk River Basin, Alaska, U.S.A., *Arc. and Alp. Res., 29*(4), 367-378, 1997.

Ng, E., and P.C. Miller. A model of the effect of tundra vegetation on soil temperatures, in *Climate of the Arctic,* edited by G. Weller and S.A. Bowling, pp 222-226, Univ. of Alaska Fairbanks, Geophys. Inst., 1974.

Ng, E., and P.C. Miller. Validation of a model of the effect of tundra vegetation on soil temperatures. *Arc. and Alp. Res., 9*(2), 89-104, 1977.

O'Neill, K., Fixed mesh finite element solution for Cartesian two dimensional phase change. *J. of Energy Resour. Technol., 105,* 436-441, 1983.

Osterkamp, T.E., and M.W. Payne. Estimates of permafrost thickness from well logs in northern Alaska, *Cold Reg. Sci. Technol, 5,* 13-27, 1981.

Ping, C. L., G. J. Michaelson, Y. Shur, and , W. M. Loya, The genesis, classification, and management of permafrost soils, in *Alaska Soil*

Geography Field Trip, NMR 495-051, 56 pp., Univ. of Alaska Fairbanks, 1994

Pradeep, P., *Modeling of the thermal processes in the arctic tundra*, M.S. thesis, 95 pp., Univ. of Alaska Fairbanks, 1994.

Price, A.G., and T. Dunne, Energy balance computations of snowmelt in a subarctic area, *Water Resour. Res., 12*(4), 686-694, 1976.

Rieger, S., D.B. Schoephorster, and C.E Furbush, *Exploratory Soil Survey of Alaska*, 213 pp., USDA Soil Conserv. Serv., Washington D. C., 1979.

Rovansek, R.J., L.D. Hinzman, and D.L. Kane, Hydrology of a tundra wetland complex on the Alaskan arctic coastal plain. *Arc. and Alp. Res., 28*(3), 311-317, 1996.

Szeicz, G , E. Gabriella, and S. Tajchman, Aerodynamic and surface factors in evaporation, *Water Resour. Res., 5*(2), 380-394, 1969.

Vourlitis, G L., and W. C. Oechel Eddy covariance measurements of net CO^2 flux and energy balance of an Alaskan moist-tussock tundra ecosystem, *Ecology*, in press, 1998.

Waelbroeck, C , Climate-soil processes in the presence of permafrost: a systems modeling approach *Ecol. Model., 69,* 185-225, 1993.

Waelbroeck, C., P. Monfray, W.C. Oechel, S. Hastings, and G. Vourlitis, The impact of permafrost thawing on the carbon dynamics of tundra, *Geophys. Res. Lett., 24*(3), 229-232, 1997.

Wilmott, C. J., and D.E. Wicks, An empirical method for the spatial interpolation of monthly precipitation within California, *Phys Geogr., 1,* 59-73, 1980.

Zhang, Z., D.L. Kane, and L.D. Hinzman, Development and application of a spatially distributed arctic thermal and hydrologic process model, *Int. J. Hydrol. Process*, in press, 1998.

Zarling, J.P., W.A. Braley, and C. Pelz, The modified Berggren method--A review, in Proceedings of the Fifth International Conference on Cold Regions Engineering, pp. 263-273, Am. Soc. of Civ. Eng., New York, 1989.

L.D. Hinzman, D.J. Goering and D.L. Kane, Water and Environmental Research Center, University of Alaska Fairbanks, P.O. Box 755860, Fairbanks, Alaska 99775-5860. (e-mail: ffldh@uaf.edu; ffdjg@uaf.edu; ffdlk@uaf.edu)

(Received August 8, 1997; revised May 1, 1998;
accepted May 8, 1998.)